Convective heat transfer characteristics within a multi-package during precooling

Ahmad Nasser Eddine, Steven Duret, D. Flick, J. Moureh

▶ **To cite this version:**

Ahmad Nasser Eddine, Steven Duret, D. Flick, J. Moureh. Convective heat transfer characteristics within a multi-package during precooling. Journal of Food Engineering, 2023, 359, pp.111710. 10.1016/j.jfoodeng.2023.111710 . hal-04192381

HAL Id: hal-04192381
https://hal.science/hal-04192381v1

Submitted on 1 Sep 2023

HAL is a multi-disciplinary open access archive for the deposit and dissemination of scientific research documents, whether they are published or not. The documents may come from teaching and research institutions in France or abroad, or from public or private research centers.

L'archive ouverte pluridisciplinaire **HAL**, est destinée au dépôt et à la diffusion de documents scientifiques de niveau recherche, publiés ou non, émanant des établissements d'enseignement et de recherche français ou étrangers, des laboratoires publics ou privés.

Public Domain

Convective heat transfer characteristics within a multi-layer packaging: application on a pallet of strawberries

Ahmad Nasser eddine*[(a)], Steven Duret[(a)], Denis Flick[(b)], Jean Moureh[(a)],

[(a)] Université Paris-Saclay, INRAE, FRISE, 92761 Antony, France

[(b)] Université Paris-Saclay, INRAE, AgroParisTech, UMR SayFood, 91120 Palaiseau, France

* **Corresponding author:** ahmad.nasser-eddine@inrae.fr

Abstract

Convective heat transfer coefficients (CHTC) on the external sides of a strawberry airtight clamshell (AC) in a pallet were characterized. The CHTCs were measured on the five sides of one instrumented AC. The instrumented AC was then displaced at different positions in two trays representing a half level of a pallet to characterize the corresponding CHTCs. These measurements were performed on four tray designs. The experimental results showed different levels of heterogeneity: along the airflow direction, in the width positions, and between the different sides of the AC. By comparing the performance of different designs, it was found that adding vent holes to the trays improves the average CHTC within the trays but increases the heterogeneity between the different sides of one AC. By contrast, increasing the air headspace height above the AC leads to lower but more uniform CHTC values between the different positions. Based on the effect of mixed convection on the heat transfer, dimensionless correlations related to CHTC were proposed between Nusselt, Reynolds and Rayleigh numbers. Similarly, a 3D CFD model was developed on ANSYS-Fluent code to predict CHTC on the different packaging sides within the trays. A good agreement was found between numerical and experimental values (mean relative error < 20%).

Keywords: Cold chain, Modified atmosphere package, Multi-layer package, Convective heat transfer coefficient, Experiments, CFD

Nomenclature

q	heat transfer rate, W
A	area, m^2
h	convective heat transfer coefficient, $W.m^{-2}.K^{-1}$
T	temperature, K
D	diameter, m
u	velocity, $m.s^{-1}$
g	gravity acceleration, $m.s^{-2}$

Dimensionless groups

Nu	Nusselt number
Re	Reynolds number
Pr	Prandtl number
Gr	Grashof number
Ra	Rayleigh number

Superscripts and subscripts

avg	average
max	maximum
min	minimum
a	air
s	surface
num	numerical
exp	experimental
o	orifice
f	flux-meter

Acronyms and abbreviations

CFD	computational fluid dynamics
MAP	modified atmosphere packaging
AC	airtight clamshell
CHTC	convective heat transfer coefficient, $W.m^{-2}.K^{-1}$
TD	tray design
TOA	total opening area
RMSE	root-mean-square error

Greek letter

ν	kinematic viscosity, $m^2.s^{-1}$
λ	thermal conductivity, $W.m^{-1}.K^{-1}$
ε	turbulent dissipation rate, $m^2.s^{-3}$

k	turbulent kinetic energy, $m^2.s^{-2}$
β	thermal expansion, K^{-1}
α	thermal diffusivity, $m^2.s^{-1}$

1. Introduction

Strawberries represent one of the most popular and desirable fruits due to their appearance and their nutritional content (Almenar et al., 2007). However, they are highly perishable as they are susceptible to mechanical damage, water loss, decay, and physiological deterioration (Anderson et al., 2004).

Packaging plays an important role into ensuring functions like containment, protection, storage, and distribution of horticultural products (Mukama et al., 2020). Moreover, it helps in maintaining optimal conditions (temperature and humidity) for products in order to preserve their quality and extend their shelf life. Strawberries are usually packed into multi-layer of packaging. First, clamshells are used as primary packaging and placed into trays. Different types, dimensions, and materials of clamshell are used (Schudel et al., 2022). The most commonly used packages are vented clamshells made of polyethylene terephthalate (PET) (Shrivastava et al., 2023).

Several studies were carried out to study the effect of different designs of PET clamshells and trays (Anderson et al., 2004; Ferrua and Singh, 2011; Nalbandi et al., 2016). The characteristics of the primary (clamshells) and secondary (trays) packaging have an impact on the cooling rate and uniformity and should be designed together to improve the performance of the cooling (Anderson et al., 2004). Ferrua and Singh (2011) proposed an alternative package design to increase the homogeneity of strawberries temperature inside the clamshell and between the clamshells at different positions. Most of these studies focused on the products temperature evolution in the packages only during the precooling process. Schudel et al. (2022) compared

the performance of clamshell designs on strawberries quality during a whole cold chain from farm to retailer.

For fruits like strawberries, maintaining an appropriate low temperature is not a sufficient condition; controlling CO2 and O2 levels and humidity inside the clamshell can increase the shelf life throughout the post-harvest chain by reducing the heat of respiration. In this context, modified atmosphere packaging (MAP) is considered a promising technology.

The majority of the studies considered one single airtight clamshell and focused on the impact of CO2 and O2 concentration, storage temperature and humidity, headspace and fruit number on the strawberries mass loss and shelf life (Bovi et al., 2018; Joshi et al., 2019; Matar et al., 2018; Sousa-Gallagher and Mahajan, 2013). These studies took into account the effect of product respiration rate and package permeability to CO2, O2 and H_2O on metabolic activity and deterioration of the food product.

However, in the case of MAP, heat transfer is limited by the airtight packaging, therefore, the product temperature evolution is highly dependent on the convective heat transfer coefficient (CHTC) on the packaging walls. In a pallet, the CHTC is heterogeneous and is mainly influenced by the airflow. Therefore, secondary packaging (tray) characteristics and clamshell arrangement within the trays become critical factors to the CHTC as they directly affect the local airflow characteristics around packages which in turn affect the atmosphere conditions within the airtight clamshells (AC) via transfer mechanisms through AC walls (Nasser Eddine et al., 2022).

CHTC is one of the performance parameters used to understand the effect of the packaging design or staking patterns on cooling performance and heterogeneity of individual packages (Berry et al., 2016; Berry et al., 2017; Defraeye et al., 2014; Defraeye et al., 2013; Wu et al., 2018). In these studies, the CHTC was predicted using a CFD model and applying a steady state method. Other studies used experimental methods to analyze the CHTC on the surface of

different products using transient (Dincer, 1994) or steady state (Merai et al., 2019; Willix et al., 2006) methods.

However, to our knowledge, the CHTC on the wall of airtight clamshells placed in a pallet were characterized neither experimentally nor numerically, although their impact on the product temperature and quality evolution.

The aim of this study was to measure the CHTC on the different sides of an airtight clamshell (AC) inside a tray of a ventilated pallet. Measurements were carried out on different AC positions inside the trays representing a pallet level. Four different tray characteristics were studied. This makes it possible to evaluate the cooling performance of different tray designs in terms of CHTC levels and heterogeneity.

The analysis of experimental results also allowed to derive a relationship between the local heat transfer coefficient and the airflow in the main orifice supplying the tray.

Another overall objective of this study is to assess the ability of CFD approach to predict local airflow and heat transfer mechanisms around ACs in a pallet. After adequate validation, the CFD model could be used as a design tool to optimize clamshells and trays in order to improve the cooling processes of products, reducing the need for expensive and time-consuming experiments.

This study, focused on CHTC, is part of a research project whose objective is to predict the evolution of the product (strawberries) in terms of temperature, water content and quality along the cold chain using MAP. The next step is the experimental and numerical characterization of the heat and mass transfer at the scale of a clamshell. For this step, the knowledge of the CHTC on the different wall sides is essential, especially, for weight loss and condensation issues. For example, if the product is warmer than the blown air, the product is expected to dehydrate and the produced water vapor to condense on the internal wall of highest CHTC. Further CO_2 and

O_2 transfers and product metabolism will be integrated in the model to predict quality evolution and remaining shell life.

2. Materials and methods

2.1. Experimental setup

For the purpose of this study, empty airtight clamshells (AC) were used. Due to the symmetric arrangement of the trays on a pallet layer, the experimental setup represented half of a layer, i.e. 2 trays were considered (Figure 1). Each tray contained 16 ACs.

The experimental setup was built inside a room where the temperature can be controlled and set at 15°C. The setup consists of a rectangular duct (Tunnel) with, successively, an inlet section, a middle section containing the packaging, an outlet section (Figure 1a). Two transparent poly-(methyl-methacrylate) (PMMA) trays with 583 mm x 370 mm x 100 mm as internal dimensions and 593 mm x 380 mm x 105 mm as external dimensions (Figure 1-b) were placed in series inside the tunnel (middle section). Figure 1c represents the external dimensions of the AC used. The AC's were arranged in a pattern to allow a regular 4 mm air gap between the AC edges in the transversal direction and a 2 mm air gap along the airflow.

Two fans (RS PRO 24 V DC) fixed at the outlet section create a differential pressure between the inlet and the outlet to let the air flow through the packages. The power supplied to the fans was regulated to ensure the desired air speed at the tunnel entrance. The system was sealed to ensure no infiltrations. A honeycomb was placed at the inlet of the tunnel to further stabilize the airflow.

2.2. Tray designs

Performances of an actual open-top tray design called TD1 is compared to three alternative designs (TD2, TD3, and TD4). These alternatives are proposed to evaluate the effect of additional orifices and air gap above the ACs on the heterogeneity of heat transfer coefficients around packages. The actual design (TD1) used in the market has a lateral trapezoidal orifice

with a 5 mm air gap above the ACs. TD2 is similar in size to TD1, the only difference is that circular vent holes with a diameter of 30 mm have been added to the longitudinal face of the tray (Figure 2). In the case of TD3 and TD4, the height has been increased to 128 mm to provide a larger air gap (28 mm).

The different tray designs were evaluated and compared under the same airflow rate. In the case where each clamshell would contain 250 g of strawberries, the chosen reference airflow rate per unit of fruit mass would be 1.1 $L.s^{-1}.kg^{-1}$. The air velocity at the inlet of the tunnel leading to the ventilated trays was measured using an LDV device (Dantec FlowExplorer-2D), in order to calculate the inlet airflow and to ensure that the same airflow rate is flowing through the different package designs.

2.3. Convective heat transfer coefficient measurements

The method used to measure the local CHTC on the surfaces of the AC is similar to that applied in previous studies (Merai et al., 2019; Willix et al., 2006). A circular (30 mm diameter) copper-surface heat flux sensor (Captec-France) with a heating resistance bonded to the surface of the flux-meter was used (Figure 3a). The calibrated accuracy of the flux-meter is assured by the manufacturer to 3% of the read value. A specific value obtained for each heat flux sensor makes it possible to convert the output signal from μV into $W.m^{-2}$. Five sides of one instrumented AC were equipped with heat flux sensors and thermocouples. The CHTC for each side is calculated using the measured heat flux and the recorded temperature difference between the surface of the flux-meter and the surrounding air according to Newton's law:

$$q/A = h(T_s - T_{air}) \quad (1)$$

Temperatures were measured using T-type thermocouples with a precision of ± 0.1 K after individual calibration. The air temperature was measured in the tunnel before the trays (inlet section). A thermocouple was bonded between the AC surface and the heating resistance as shown in Figure 3b. The measured temperature: $T_{measured}$ is slightly higher than at the surface of

145 the flux-meter. Some experiments were conducted to determine this small difference (by adding
146 a thermocouple at the surface of the flux-meter). This allowed to establish an empirical
147 correlation (eq. 2) which takes into account the heat transfer conductance through the flux-
148 meter and the heating flux. This correlation was used to calculate the temperature of the surface
149 of the flux-meter T_s (surface exposed to airflow).

$$T_s = T_{measured} - \frac{q}{h'A} \text{ with } h' = 240 \text{ W.m}^{-2}\text{.K}^{-1} \quad (2)$$

150 Considering the symmetry of the packaging system, the measurements were conducted on half
151 of the tray (highlighted in yellow in the Figure 3c). The instrumented AC was displaced at
152 different positions into the tray in order to characterize the corresponding CHTC. Figure 3c
153 shows the numbering of the AC positions inside the two trays and the names of the different
154 sides.
155 Each experiment consisted in heating continuously the resistance until a steady state was
156 reached. The time to reach a constant temperature depended on the side and the position of the
157 AC. It varied between 30 minutes and 420 minutes. Each run measured the CHTC on fives
158 sides of one AC position. Temperature and flux-meter output signal acquisitions were
159 performed every 10 s using a data-logger (Keysight DAQ970A) and acquisition software
160 (Keysight BenchVue).
161 **Evaluation of CHTC heterogeneities**
162 Several average CHTC levels and heterogeneity indicators were defined to compare the
163 performance of different tray designs. These functions were calculated from the measurements
164 made on each surface of the AC and at the 16 different positions (index i):

Average CHTC for vertical sides of AC at position i

$$CHTC_{avg.vert.i} = \frac{CHTC_{right.i} + CHTC_{back.i} + CHTC_{left.i} + CHTC_{front.i}}{4} \quad (3)$$

Average CHTC of the five sides of AC at position i

$$\mathrm{CHTC_{avg.i}} = \frac{\mathrm{CHTC_{right.i}} + \mathrm{CHTC_{back.i}} + \mathrm{CHTC_{left.i}} + \mathrm{CHTC_{front.i}} + \mathrm{CHTC_{top.i}}}{5} \quad (4)$$

Overall CHCT average of all AC in the trays

$$\mathrm{CHTC_{avg}} = \frac{\sum \mathrm{CHTC_{avg,i}}}{16} \quad (5)$$

Deviation of the $\mathrm{CHTC_{avg.i}}$ from the overall average (Position Heterogeneity Index)

$$\mathrm{PHI_i} = \frac{\mathrm{CHTC_{avg,i}} - \mathrm{CHTC_{avg}}}{\mathrm{CHTC_{avg}}} \quad (6)$$

Maximal difference of the CHTC between the different sides of AC at position i (Side Heterogeneity Index)

$$\mathrm{SHI}_i = \frac{\mathrm{CHTC_{max.i}} - \mathrm{CHTC_{min.i}}}{\mathrm{CHTC_{avg.i}}} \quad (7)$$

Standard deviation

$$\mathrm{SD} = \sqrt{\frac{\sum(\mathrm{CHTC_{avg.i}} - \mathrm{CHTC_{avg}})^2}{16}} \quad (8)$$

2.4. Relationship between local heat transfer coefficient and airflow in the orifice

A series of CHCT measurements for two AC positions inside tray design (TD1) were carried out with different airflow rates and different heating powers. In order to develop a dimensionless correlation, a Reynolds number based on the hydraulic diameter of the trapezoidal orifice and the average velocity in this orifice was defined. The Nusselt and Rayleigh numbers were based on the diameter of the flux-meter. The Reynolds and Rayleigh number varied respectively in range [0, 3700] and [4000, 14000]. The two AC positions 9 and 12 were chosen because they have the highest and lowest average CHTC respectively.

$$\mathrm{Nu} = \frac{\mathrm{h} \times \mathrm{D_f}}{\lambda_a} \quad (9)$$

$$\mathrm{Re} = \frac{\mathrm{u} \times \mathrm{D_o}}{\nu} \quad (10)$$

$$\mathrm{Ra} = \frac{\mathrm{g}\beta(\mathrm{T_s} - \mathrm{T_a})\mathrm{D_f}^3}{\nu\alpha} \quad (11)$$

Due to low velocity at some positions, free convection cannot be ignored. Therefore, a mixed convection correlation was proposed, in the form:

$$\mathrm{Nu} = \varphi \mathrm{Re}^{\beta} + \delta \mathrm{Ra}^{\gamma} \quad (12)$$

with φ, β, δ, γ coeffcients to be determined.

2.5. Numerical simulations

A three-dimensional model was developed to predict the CHTC on the surfaces of the AC placed inside the two trays using the CFD code ANSYS 21.R1. Only half of the trays was modeled based on the assumption that the packaging system is symmetric. The experimental geometry was reproduced using SpaceClaim 2021.R1. The computational domain is composed of the free airflow fluid zone and the solid tray zones. The AC walls are modeled as surfaces with no thickness. Conditions of no-slip are assumed at the surfaces of the trays and AC walls. A circular surface representing the surface of the flux-meter was created on each side of the AC. The model was applied for two configurations TD3 and TD4.

A hybrid mesh (tetrahedral and hexahedral cells) was created for the numerical study with 7.3×10^6 cells for TD3 and 7.4×10^6 cells for TD4.

The inlet boundary condition was defined as velocity inlet and set to the value measured by the LDV. The temperature at the inlet was set to 15°C, as the experimentally measured temperature. The outlet boundary condition was set to the atmospheric pressure.

With regard to the thermal conditions of the circular surfaces added to the sides of the AC, two approaches were performed:

1- Considering that the type of convection is mixed inside the tray, therefore, buoyancy effect was taking into account in the momentum equation in order to model heat transfer by natural convection. In this case, to calculate the CHTC of each side for a particular AC position, the heat fluxes of each side that were found experimentally at steady state were imposed to its corresponding circular surfaces.

2- Assuming that the forced convection is predominant in all zones inside the trays. Accordingly, buoyancy effect was not considered. In this case, a fixed temperature (20°C) was imposed to the circular surface of each side for a particular position.

In total 16 steady-state simulations were run to obtain the CHTCs of the different sides for the different positions.

Regarding the turbulence model, Realizable k-ε model with enhanced wall treatment was applied in this study. The SIMPLE algorithm with second-order upwind technique is applied to solve the pressure-velocity-temperature coupled equations.

Simulations were run using a computer with 2.4 GHz Intel® Xeon® Silver 4210R CPU and 256 GB of RAM.

The validity of the model under the two approaches was evaluated by comparing the CHTC values obtained from models to the CHCT measurements performed experimentally using the root-mean-square error (RMSE); for side k:

$$RMSE = \sqrt{\frac{1}{16}\sum_{i=1}^{16}(CHTC_{k.i.num} - CHTC_{k.i.exp})^2} \quad (13)$$

3. Results and discussion

3.1. CHTC levels and heterogeneities

Figure 5 represents the heat transfer heterogeneities inside the different tray designs, by displaying the different indicators defined above in paragraph 2.4. These results were obtained for the reference airflow rate: 8.8 $L.s^{-1}$ (1.1 $L.s^{-1}.kg^{-1}$ on the basis of 250 g/AC). For tray design 1 (TD1) this corresponds to an average air velocity in the trapezoidal orifice of 0.9 $m.s^{-1}$ and a Reynolds number of 3700. The temperature difference between the flux-meter and the air was kept between 2 and 4 K (by adjusting the heating power) in order to minimize free convection. For example, concerning the bottom right AC (n°2) for the tray design 1 (TD1)

$CHTC_{avg.i}$ =18, $CHTC_{top.i}$ = 11, $CHTC_{avg.vert.i}$ =20 means that the side-averaged CHTC (average over the 5 sides) for this AC is 18 $W.m^{-2}.K^{-1}$, the top wall CHTC is only 11 $W.m^{-2}.K^{-1}$ and on the vertical sides walls it is averagely 20 $W.m^{-2}.K^{-1}$.

SHI_i =0.79 (Side Heterogeneity Index) means that the difference between highest and lowest CHTC on the 5 sides of this AC is 79% of the side-averaged value.

PHI_i = -0.15 (Position Heterogeneity Index) means that this AC has a side-averaged CHTC 15% lower than the overall CHTC (for all the sides of all the ACs).

Regarding the actual tray design TD1, the most important heterogeneity is found in the width positions (transversal direction) for the two trays. The ACs placed in the middle (near the symmetry plane) have $CHTC_{avg.i}$ from 23 to 35 $W.m^{-2}.K^{-1}$ and those at the border only from 14 to 18 $W.m^{-2}.K^{-1}$. The highest $CHTC_{avg.i}$ is 2.5 times higher than the lowest. The variations of the CHCT are mainly related to the characteristics of the airflow. Therefore, the heterogeneity can be explained by the fact that the ACs positioned at the border are less ventilated since most of the airflow passes in the middle of the tray downstream of the vent hole (Figure 1b). Second and third column of Figure 5 reflects the effect of the airflow behavior on the heat transfer of different sides. Comparing the CHTC of the top wall between the ACs placed in the middle and those placed at the border, a maximal difference of 31 $W.m^{-2}.K^{-1}$ can be observed between the AC 9 and AC 10. This difference can be explained by the fact that AC 9 is located in the core air jet flowing through the vent hole of the tray while AC 10 is located in a supposed weakly ventilated recirculation area induced by the same jet. In this configuration, there is a primary airflow represented by an air-jet issuing the vent hole that develops in the air headspace above the ACs. The secondary airflow passing between the ACs also results in a significant heterogeneity between the $CHTC_{avg.vert.i}$ of the ACs positioned in the middle and those placed at the border where a maximum difference of 17 $W.m^{-2}.K^{-1}$ can be observed between the AC 1 and AC 6.

A second heterogeneity can be noticed between the different sides of each AC especially for positions 7 and 10 as the relative difference between the maximum and minimum CHTC on the same AC reaches about 100% (1.00 for position 7 and 1.02 for position 10). The thermal behavior of the AC 7 can be explained by the fact that it is placed near the outlet of the first tray, the flow is accelerating towards the vent hole. Therefore, the right, left, back, and top side are subjected to higher velocities compared to the front side where it is facing a relatively dead zone, which has resulted in a higher CHTC on different sides except the front side.
A small heterogeneity is found along the flow direction: The CHTC is higher near the inlet and outlet sections of the trays where the airflow accelerates when passing through the opening.

3.2. Influence of tray design on CHTC level and homogeneity

Adding vent holes in TD2 in comparison to TD1 has increased the overall averaged CHTC from 21 to 24 $W.m^{-2}.K^{-1}$ (Table 1). This increase concerns both top and vertical sides. Moreover, on the top, the CHTC values become less heterogeneous between middle and border lines ACs. Therefore, this leads to a better global homogeneity: the maximum PHI decreases from 0.64 for TD1 to 0.40 for TD2. Locally, the major improvements were seen on the ACs positioned near the added vent holes (AC n°1-2-7-8-9-10-15-16) as it can be noticed in Figure 5. However, it should be noted that the heterogeneity between the different sides of each AC increased. The relative difference between the maximum and minimum CHTC (SHI) for AC 10 increased from 1.02 to 1.5 (Figure 5). This can be explained by the fact that the CHTC of the front side significantly increased due to its position in front of the added vent hole (outlet of tray 1 and inlet of tray 2) contrary to the CHTC of back side. Figure 6 presents boxplots showing the dispersion of the CHTC values on each side under different packaging designs. By comparison with TD1, the dispersion observed for TD2 is smaller at top but larger at the front which confirms previous remarks.

Comparing the tray designs in terms of air headspace above the ACs, the results show that TD3 when compared to TD1 has lower CHTC values with similar difference between the ACs placed in the middle and at the border (higher in the middle). This could be explained by the effect of the higher headspace of TD3 compared to TD1 implying lower velocity magnitude above the ACs (for the same flow rate) and therefore lower CHTC values for top values on the whole tray. Due to this airflow behavior, the heterogeneity between the different sides is high in the middle, SHI reaches 1.39 for AC 1. However, the position heterogeneity is lower: the maximum PHI equals 0.37 for TD3 when it was 0.64 for TD1. Figure 6 shows that for most of the sides, the CHTC is less dispersed.

For TD4, the additional vent holes also improved the CHTC compared to TD3. The $CHTC_{avg,i}$ varied from 6 to 12 $W.m^{-2}.K^{-1}$ and from 8 to 22 $W.m^{-2}.K^{-1}$ for TD3 and TD4 respectively. As shown on figure 6, the CHTC of the front, left and right sides increased.

Such a study allows to evaluate the heat transfer characteristics of different packaging designs. It helps to identify the most sensitive areas (AC positions) inside a tray, which is essential to assess them in terms of cooling rate and fruits quality. Through this study, we observed that decreasing the air headspace height above the ACs allows higher CHTC levels for a given airflow rate. Globally, since the section is reduced, averagely the velocity is increased allowing better ventilation. The impact of additional vent holes is relevant for increasing the average heat transfer but the effect in our case remains limited. Locally, additional vent holes mainly concerns the ACs placed in front of the orifices. It is therefore worthwhile to study the effect of the position of the orifices on the performance of packaging. Moreover, a high heat transfer coefficient can lead to fast cooling, however, this is not always beneficial for the quality of the fruit. Defraeye et al. (2013) stated that the optimal packaging design in terms of cooling is not necessarily the best in terms of fruit quality. In addition, a

higher heterogeneity between the sides (higher $SHI_{i.max}$) is observed with the additional vent holes.

3.3. Nu-Re-Ra correlation

In practice, along the cold chain, the air flowrate is often much less than 1.1 $L.s^{-1}.kg^{-1}$ (our reference flowrate) and free convection can become significant or even dominant compared to forced convection. This is why the effect of air flowrate (from 0 to 1.1 $L.s^{-1}.kg^{-1}$) was studied in some positions. The experimental data obtained for ACs 9 and 12 (highest and lowest $CHTC_{avg.i}$) in Tray Design 1 (TD1) were used for the development of a correlation between Nu, Re and Ra as given in eq. (12).

The power value related to Reynold number (β) was estimated by regression using only data for which forced convection is predominant (high flow rate, low heating power). The obtained value: $\beta = 0.60$ is close to the one found by Saha et al. (2006) ($\beta = 0.65$) and Pham et al. (2019) ($\beta = 0.63$). The power value related to Rayleigh number (γ) was assumed to be 1/4 as in similar problems (Özışık, 1985).

Table 2 presents the coefficients δ and φ (for different positions). The value of δ does not depend on position because free convection is induced by the heated flux-meter, not by the local velocity due to the forced airflow. The values are close whatever the sides.

The values of φ characterize the intensity of heat transfer related to local velocity (depending on AC position and side). The values vary a lot from 0.008 to 0.364, this clearly indicates the importance of local airflow characteristics. The highest value is for the front side of AC 9 and can be explained by the fact that the front side of this AC is facing the trapezoidal orifice where a high velocity is expected. On the other hand, the back face of AC 12 is certainly in a relatively dead zone. There is no simple way to express how φ depends on the orientation and positions of the AC, this reflects a complex flow pattern as could be observed by simulation.

Figure 7 represents the Nusselt number calculated using the correlation and the experimental results for different Re. A good agreement is observed. The values observed for Re=0 correspond to pure free convection (no airflow). In the dead zones like the top side of AC 12, the CHTC increased slightly (less than 50 %) with flowrate. In contrast, in the zones where the forced convection is predominant like front, right and left sides of the AC 9, Nu rose largely (for example from around 10 to 50 when the Re increased from 0 to 3700 for the left side of AC 9).

3.4. Numerical model

Figure 8 and Figure 9 compare the experimental CHTCs and the predicted values from the numerical model (including natural convection) for TD3 and TD4.

Globally, there is a good agreement: most of the CHTCs are predicted at +/- 20%. For TD3, the model overestimated the CHTC of the top sides and underestimated the CHCT of the vertical sides, which may be due to the overestimation of the airflow through the headspace by the model.

Table 3 compares RMSE between experimental and numerical results with and without taking into account natural convection for TD3. Excepted for the top side, RMSE is lower for mixed convection. This highlights that free convection cannot be ignored especially on the side walls. Different factors influencing simulation and experiment can be responsible for the discrepancies observed in some points. For example, the actual geometry is not perfectly symmetric, the air gaps are not exactly the same, the surface of the ACs is not totally flat and smooth, and the cables can slightly modify the airflow around the ACs. Also the turbulence model and the boundary treatment are perhaps not completely appropriate notably in the zones of very low velocity (locally laminar flow).

4. Conclusion

Experiments were conducted to measure the local convective heat transfer coefficient (CHTC) of an airtight clamshell walls for different tray designs representing a half pallet level.

Two major levels of heterogeneity were identified: according to the AC position in the tray design and the considered side (top, front, back, left, and right). These heterogeneities are induced by the airflow behavior in the headspace and its diffusion between the ACs. Two main zones inside the tray are identified: the middle of the tray where the main opening is located and where high CHTCs are observed and the poorly ventilated zone at the border of the tray.

This study allowed the assessment of the effect of two factors: air headspace height and additional vent hole, on the cooling performance in terms of CHTC levels and heterogeneity. It was concluded that both of these factors should be simultaneously considered in a manner that allows for an equal airflow distribution between the headspace and the circular orifices.

The dimensionless correlation established between Nu, Re and Ra shows that free convection cannot be ignored especially on the sides placed in the poorly ventilated zone. The coefficients of this correlation depend on the side orientation and the position of the AC.

CFD model was applied to predict the CHTC on the different sides of the ACs inside the two tray designs TD3 and TD4. The numerical results of the approach using natural convection showed a better agreement with the experimental results with an overall RMSE equal to 2.2 $W.m^{-2}.K^{-1}$.

Further studies will concern experimental characterization of heat and mass transfer inside the clamshells (strawberry temperature and weight loss measurements). The modelling at the scale of a clamshell will then use the present results as boundary conditions. The difference in CHTC depending on the sides could notably determine the walls where condensation issues are probable.

5. Acknowledgements

The authors thank the French National Research Agency for the opportunity and financial support to carry out this project, under project EcoFreshChain, ANR-20-CE21-0007-01.

6. References

Almenar, E., Del-Valle, V., Hernández-Muñoz, P., Lagarón, J.M., Catalá, R., & Gavara, R. (2007). Equilibrium modified atmosphere packaging of wild strawberries. *Journal of the Science of Food and Agriculture* 87(10), 1931-1939. https://doi.org/ 10.1002/jsfa.2938.

Anderson, B.A., Sarkar, A., Thompson, J.F., & Singh, R.P. (2004). Commercial-Scale Forced-Air Cooling of Packaged Strawberries. *Transactions of the ASAE* 47(1), 183-190. https://doi.org/ 10.13031/2013.15846.

Berry, T.M., Defraeye, T., Nicolai, B.M., & Opara, U.L. (2016). Multiparameter Analysis of Cooling Efficiency of Ventilated Fruit Cartons using CFD: Impact of Vent Hole Design and Internal Packaging. *Food and Bioprocess Technology* 9(9), 1481-1493. https://doi.org/ 10.1007/s11947-016-1733-y.

Berry, T.M., Fadiji, T.S., Defraeye, T., & Opara, U.L. (2017). The role of horticultural carton vent hole design on cooling efficiency and compression strength: A multi-parameter approach. *Postharvest Biology and Technology* 124, 62-74. https://doi.org/ 10.1016/j.postharvbio.2016.10.005.

Bovi, G.G., Rux, G., Caleb, O.J., Herppich, W.B., Linke, M., Rauh, C., & Mahajan, P.V. (2018). Measurement and modelling of transpiration losses in packaged and unpackaged strawberries. *Biosystems Engineering* 174, 1-9. https://doi.org/ 10.1016/j.biosystemseng.2018.06.012.

Defraeye, T., Lambrecht, R., Delele, M.A., Tsige, A.A., Opara, U.L., Cronjé, P., Verboven, P., & Nicolai, B. (2014). Forced-convective cooling of citrus fruit: Cooling conditions and energy consumption in relation to package design. *Journal of Food Engineering* 121, 118-127. https://doi.org/ 10.1016/j.jfoodeng.2013.08.021.

Defraeye, T., Lambrecht, R., Tsige, A.A., Delele, M.A., Opara, U.L., Cronjé, P., Verboven, P., & Nicolai, B. (2013). Forced-convective cooling of citrus fruit: Package design. *Journal of Food Engineering* 118(1), 8-18. https://doi.org/ 10.1016/j.jfoodeng.2013.03.026.

Dincer, I. (1994). Development of new effective Nusselt-Reynolds correlations for air-cooling of spherical and cylindrical products. *International Journal of Heat and Mass Transfer* 37(17), 2781-2787. https://doi.org/ 10.1016/0017-9310(94)90395-6.

Ferrua, M.J., & Singh, R.P. (2011). Improved airflow method and packaging system for forced-air cooling of strawberries. *International Journal of Refrigeration* 34(4), 1162-1173. https://doi.org/ 10.1016/j.ijrefrig.2011.01.018.

Joshi, K., Tiwari, B., Cullen, P.J., & Frias, J.M. (2019). Predicting quality attributes of strawberry packed under modified atmosphere throughout the cold chain. *Food Packaging and Shelf Life* 21. https://doi.org/ 10.1016/j.fpsl.2019.100354.

Matar, C., Gaucel, S., Gontard, N., Guilbert, S., & Guillard, V. (2018). Predicting shelf life gain of fresh strawberries ' Charlotte cv' in modified atmosphere packaging. *Postharvest Biology and Technology* 142, 28-38. https://doi.org/ 10.1016/j.postharvbio.2018.03.002.

Merai, M., Flick, D., Guillier, L., Duret, S., & Laguerre, O. (2019). Experimental characterization of heat transfer inside a refrigerated trailer loaded with carcasses. *International Journal of Refrigeration* 99, 194-203. https://doi.org/ 10.1016/j.ijrefrig.2018.11.041.

Mukama, M., Ambaw, A., & Opara, U.L. (2020). Advances in design and performance evaluation of fresh fruit ventilated distribution packaging: A review. *Food Packaging and Shelf Life* 24. https://doi.org/ 10.1016/j.fpsl.2020.100472.

Nalbandi, H., Seiiedlou, S., Ghasemzadeh, H.R., & Rangbar, F. (2016). Innovative Parallel Airflow System for forced-air cooling of strawberries. *Food and Bioproducts Processing* 100, 440-449. https://doi.org/ 10.1016/j.fbp.2016.09.002.

Nasser Eddine, A., Duret, S., & Moureh, J. (2022). Interactions between Package Design, Airflow, Heat and Mass Transfer, and Logistics in Cold Chain Facilities for Horticultural Products. *Energies* 15(22). https://doi.org/ 10.3390/en15228659.

Özışık, N. (1985). *Heat Transfer: A Basic Approach*. McGraw-Hill International Editions.

Pham, A.T., Moureh, J., & Flick, D. (2019). Experimental characterization of heat transfer within a pallet of product generating heat. *Journal of Food Engineering* 247, 115-125. https://doi.org/ 10.1016/j.jfoodeng.2018.12.003.

Saha, S., Saha, G., Ali, M., & Quamrul Islam, M. (2006). Combined Free and Forced Convection Inside a Two-Dimensional Multiple Ventilated Rectangular Enclosure. *ARPN Journal of Engineering and Applied Sciences* VOL.1, NO.3, OCTOBER 2006.

Schudel, S., Shrivastava, C., Rebeaud, S.G., Karafka, L., Shoji, K., Onwude, D., & Defraeye, T. (2022). Combining experiments and mechanistic modeling to compare ventilated packaging types for strawberries from farm to retailer. *Food Packaging and Shelf Life* 34. https://doi.org/ 10.1016/j.fpsl.2022.100944.

Shrivastava, C., Schudel, S., Shoji, K., Onwude, D., da Silva, F.P., Turan, D., Paillart, M., & Defraeye, T. (2023). Digital twins for selecting the optimal ventilated strawberry packaging based on the unique hygrothermal conditions of a shipment from farm to retailer. *Postharvest Biology and Technology* 199. https://doi.org/ 10.1016/j.postharvbio.2023.112283.

Sousa-Gallagher, M.J., & Mahajan, P.V. (2013). Integrative mathematical modelling for MAP design of fresh-produce: Theoretical analysis and experimental validation. *Food Control* 29(2), 444-450. https://doi.org/ 10.1016/j.foodcont.2012.05.072.

Willix, J., Harris, M.B., & Carson, J.K. (2006). Local surface heat transfer coefficients on a model beef side. *Journal of Food Engineering* 74(4), 561-567. https://doi.org/ 10.1016/j.jfoodeng.2005.03.044.

Wu, W., Cronjé, P., Nicolai, B., Verboven, P., Linus Opara, U., & Defraeye, T. (2018). Virtual cold chain method to model the postharvest temperature history and quality evolution of fresh fruit – A case study for citrus fruit packed in a single carton. *Computers and Electronics in Agriculture* 144, 199-208. https://doi.org/ 10.1016/j.compag.2017.11.034.

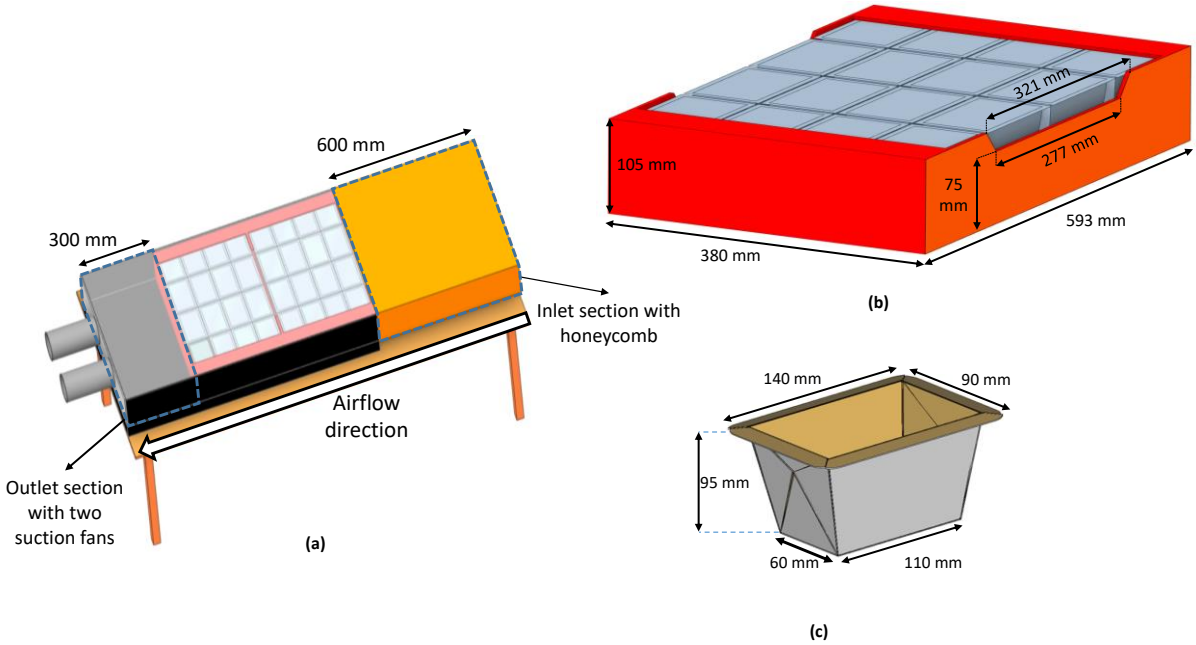

445

446 **Figure 1**: (a) Experimental setup (top view), (b) dimensions of the existing tray, (c)
447 dimensions of the AC

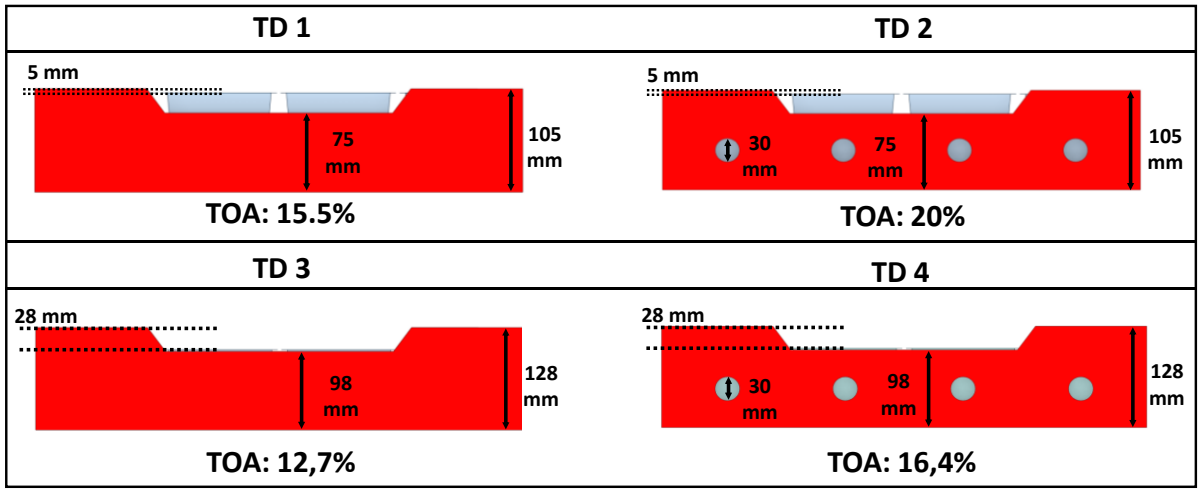

448

449 **Figure 2:** Dimensions and the total opening area (TOA) of the different tray designs

450

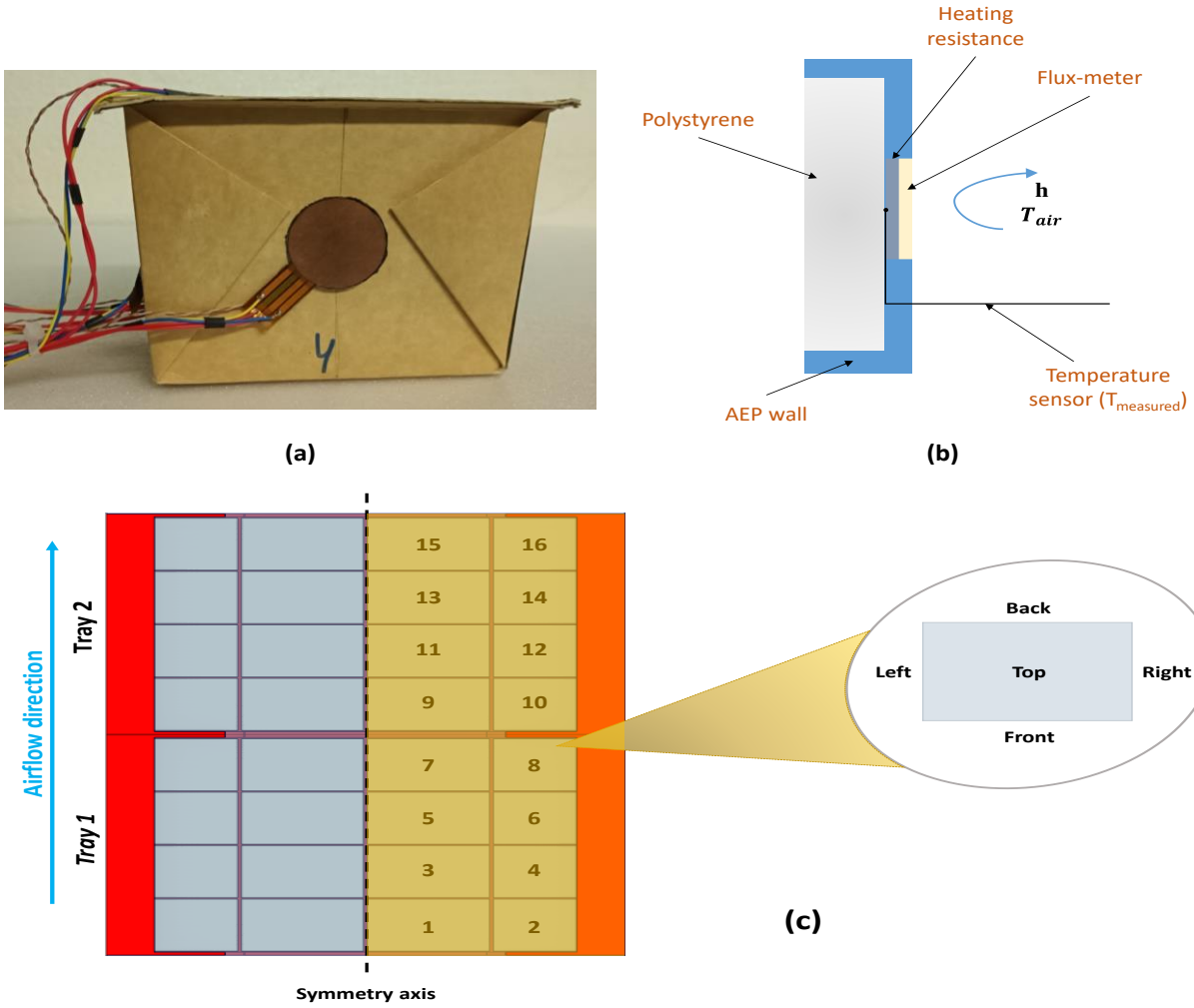

Figure 3: (a) instrumented AC with flux-meters and thermocouples, (b) schematic of a section cutting the flux-meter, (c) AC numbering and side names

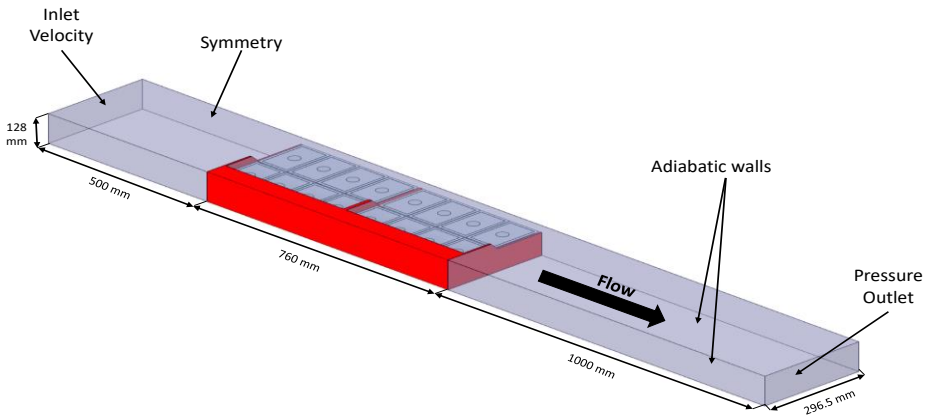

Figure 4 : CFD model boundary conditions

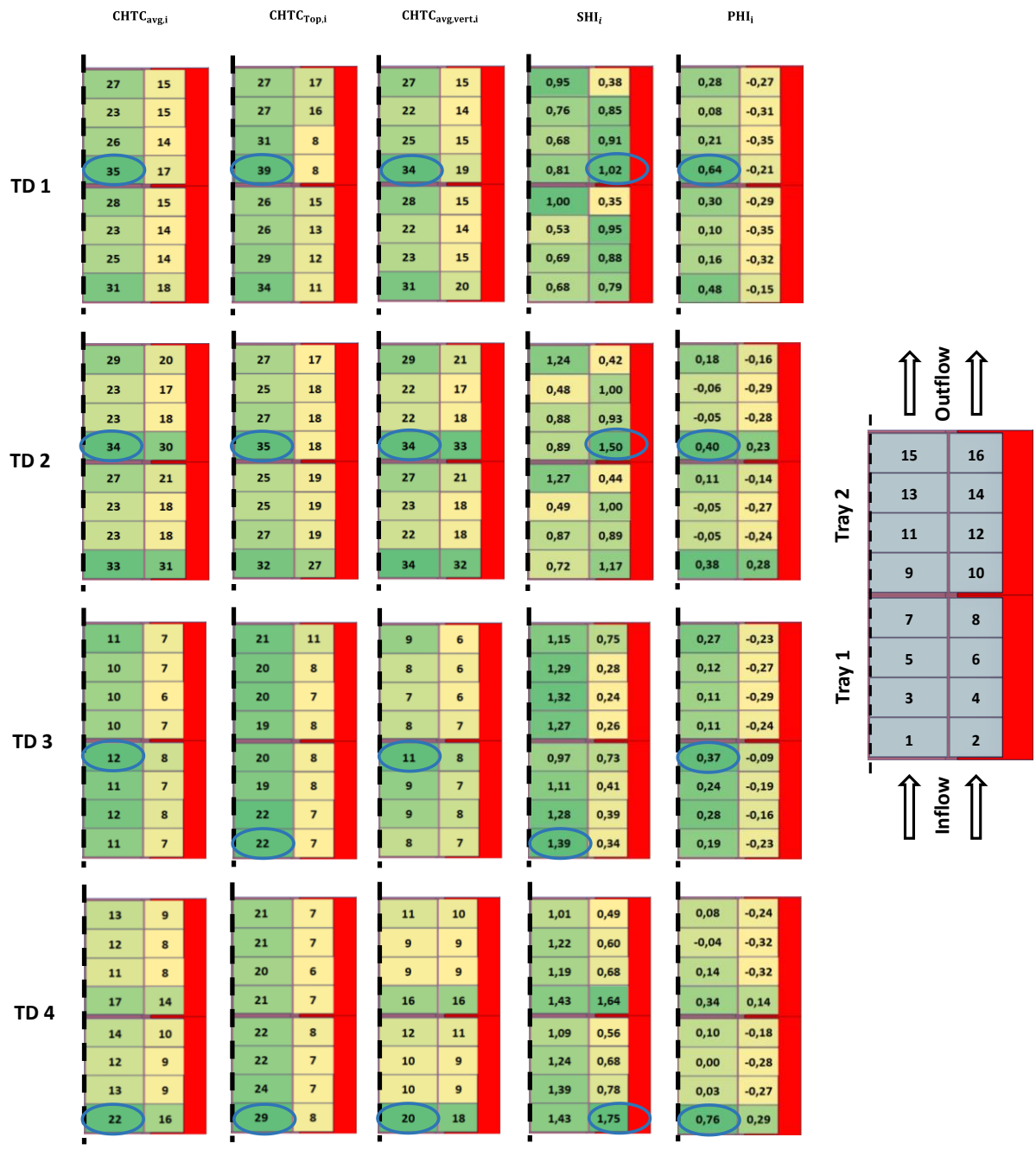

456

457 **Figure 5:** Cartographies illustrating the heterogeneities of CHTC for TD1, TD2, TD3, and
458 TD4 at 1.1 L.s^{-1}.kg^{-1}. The maximum values are circled.

459 **Table 1:** Overall average CHTCs of the ACs and their standard deviation for four tray
460 designs

	TD1	TD2	TD3	TD4
CHTC$_{avg}$ (W.m^{-2}.K^{-1})	21	24	9	12
SD (W.m^{-2}.K^{-1})	9	10	4	7

461

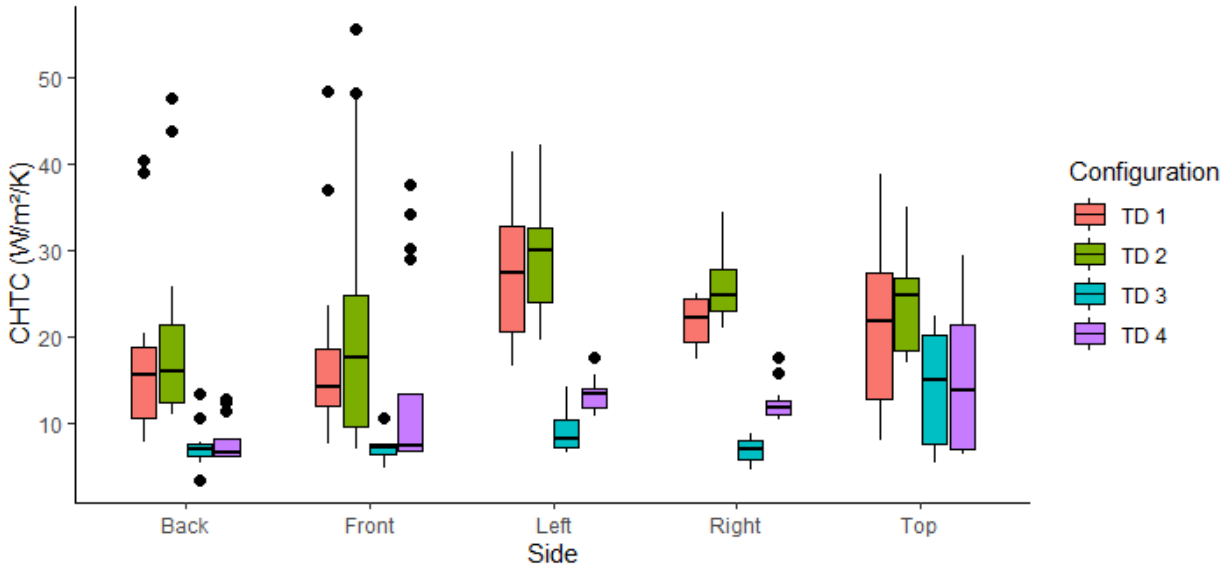

Figure 6: Boxplots showing the dispersion of the CHTC values on each side under different packaging designs. Outliers are represented by black points

Table 2: Coefficients φ and δ in Nu-Re-Ra correlation for different sides of two positions 9 and 12

	Position	**Right Side**	**Back Side**	**Left Side**	**Front Side**	**Top Side**
δ	9,12	0,685	0,761	0,824	0,790	0,800
φ	9	0,147	0,106	0,279	0,364	0,284
	12	0,138	0,008	0,125	0,046	0,020

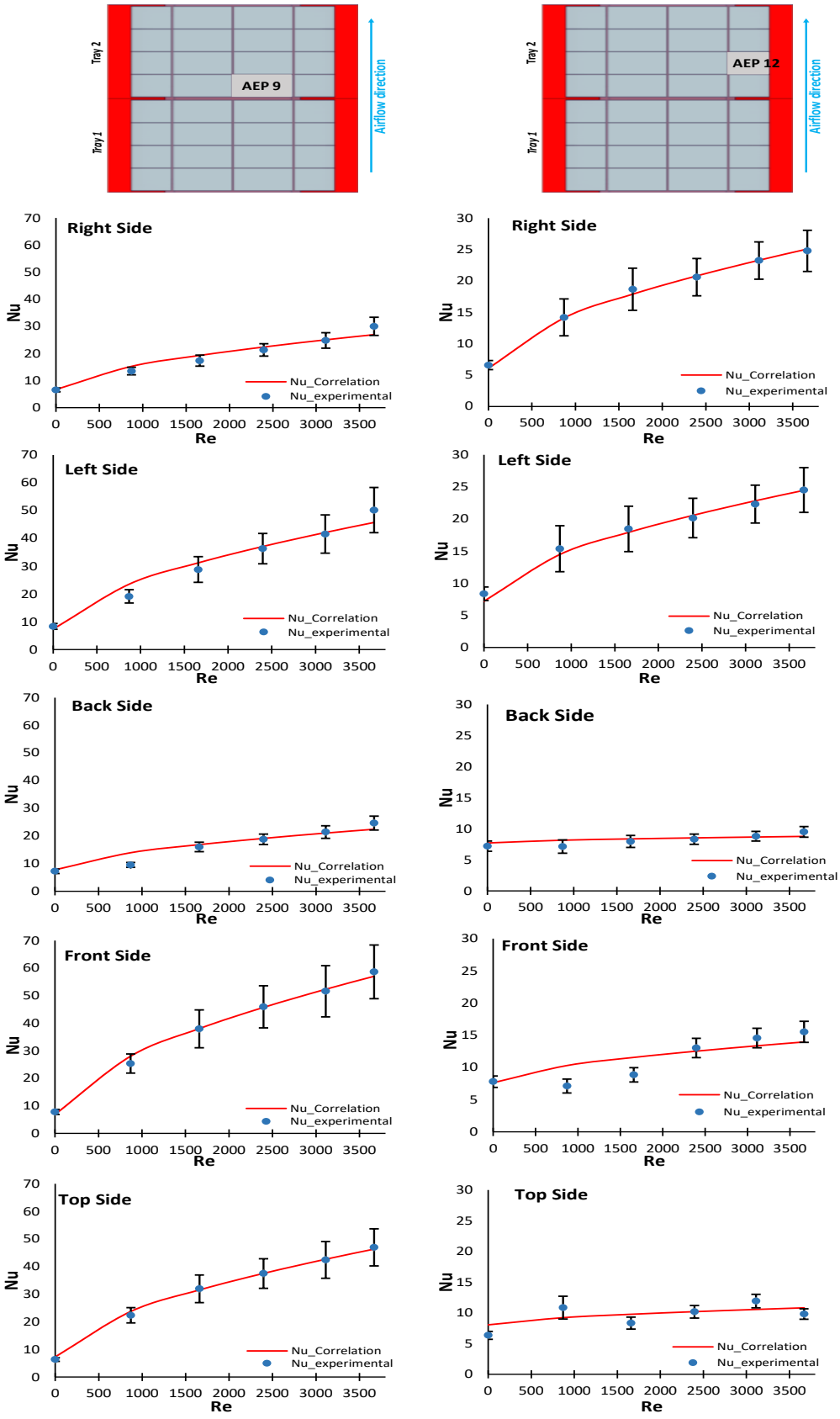

Figure 7: Nu for each sides of AC 9 and 12 as function of Re (at the orifice) for the actual tray design (TD1). The bars represent the uncertainty of measurements.

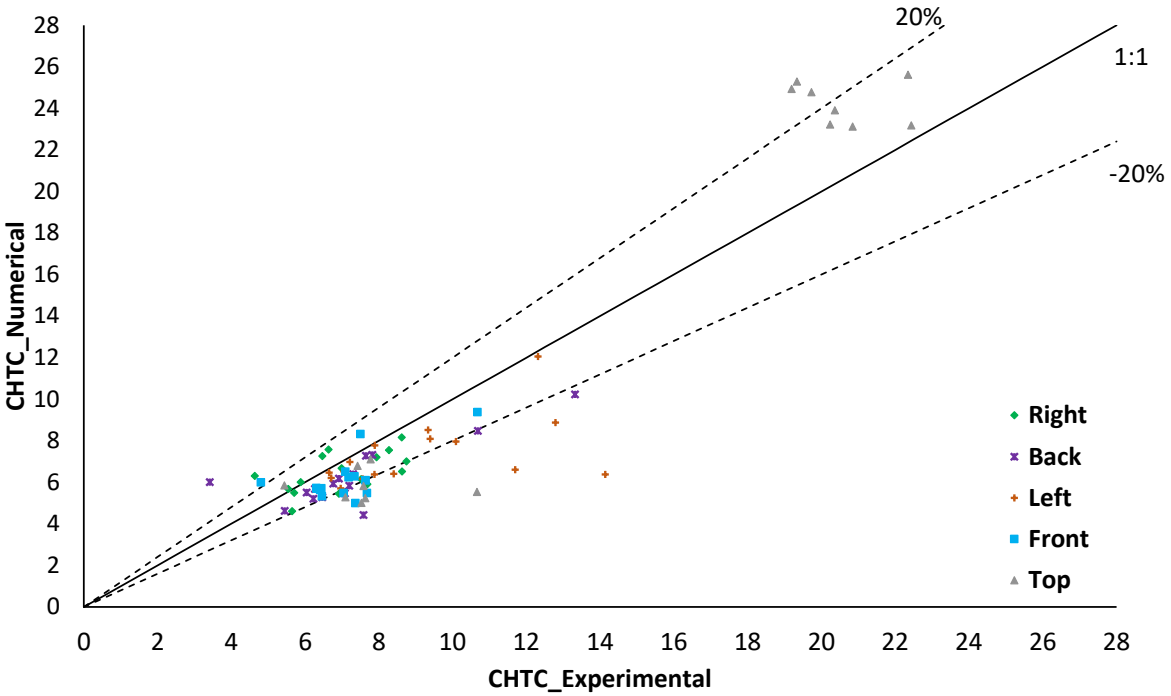

Figure 8: Comparison of the CHCT obtained from the experimental data and from the numerical model (the effect of natural convection is included) for all sides of ACs placed inside TD 3

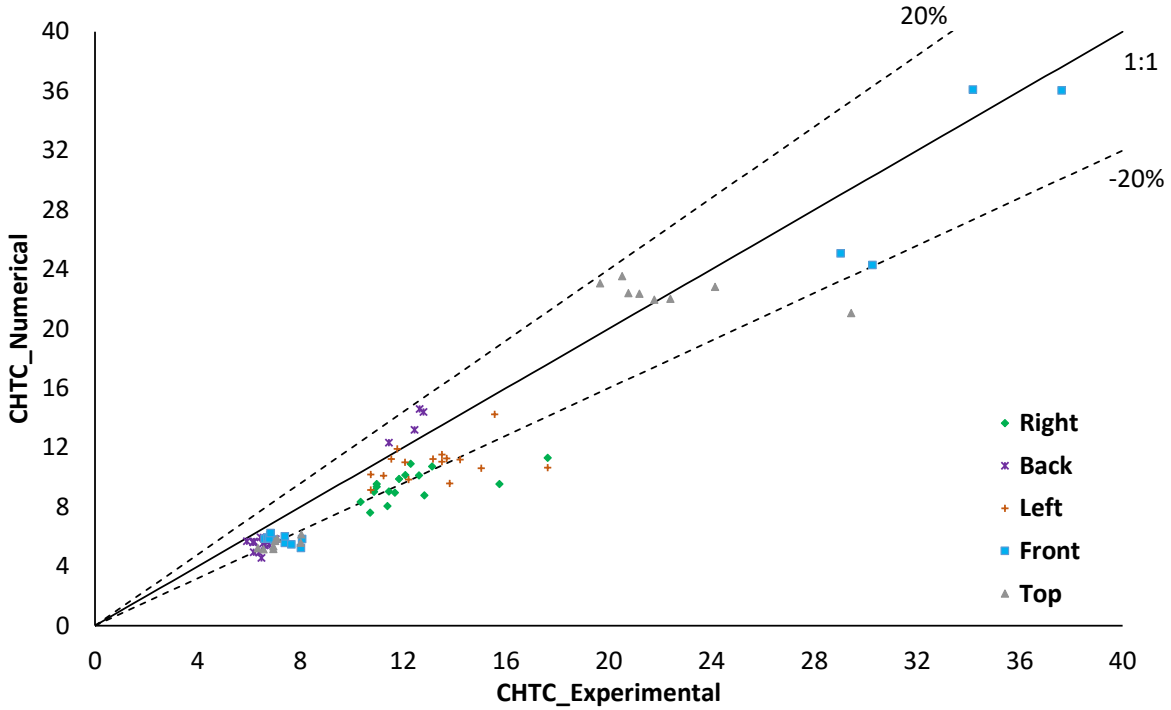

Figure 9: Comparison of the CHCT obtained from the experimental data and from the numerical model (the effect of natural convection is included) for all sides of ACs placed inside TD 4

480 **Table 3:** Results for RMSE ($W.m^{-2}K^{-1}$) for tray design TD 3

	Right	**Back**	**Left**	**Front**	**Top**	**Overall**
Experiments vs model with Forced convection	1,9	2,8	3,6	2,9	2,6	2,8
Experiments vs model with Mixed convection	1,1	1,5	2,8	1,3	3,3	2,2

481